ISSN 0022-4766, Journal of Structural Chemistry, 2019, Vol. 60, No. 7, pp. 1043-1051. © Pleiades Publishing, Inc., 2019.
Russian Text © The Author(s), 2019, published in Zhurnal Strukturnoi Khimii, 2019, Vol. 60, No. 7, pp. 1091-1099.

XPS STUDY OF THE PROCESS OF HgCdTe OXIDATION IN A GLOW DISCHARGE OXYGEN PLASMA

E. R. Zakirov[1]* V. G. Kesler[1]

Initial stages of HgCdTe oxidation in a glow discharge plasma in O_2 atmosphere are first studied using the XPS method. The chemical composition of the growing native oxide layer is investigated and the oxidation kinetics is revealed. It is experimentally established that the mechanism of HgCdTe oxidation changes as the oxide thickness reaches 2-3 nm due to the change of the limiting stage of the chemical reaction. The composition of the formed oxide is varies with depth and is characterized by low mercury content. It is suggested that the diffusion of oxygen to the oxide–semiconductor interface and its predominant interaction with tellurium are the main mechanism of the native MCT oxide growth, so that the oxide region bordering the substrate is ~10% oxygen depleted. The obtained results are discussed and compared with previously reported data on MCT oxidation in RF plasma and in liquid electrolytes.

DOI: 10.1134/S0022476619070047

Keywords: cadmium mercury telluride, ultrathin native oxide, oxidation kinetics.

INTRODUCTION

A ternary semiconducting compound mercury–cadmium–tellurium (MCT, $Hg_{1-x}Cd_xTe$) is a widely used and promising material of infrared technology. Its distinctive feature is the possibility to change the band gap in the range of 0-1.6 eV by varying the composition x; therefore, it can be used to create photodetectors that are sensitive to the radiation both in the near- and in the far-IR regions. Besides, an extremely small change in the lattice constant (the difference between HgTe and CdTe lattice parameters is 0.4%) allows fabricating multi-color IR photodetectors. High-speed work results from significant mobility of charge carriers, and high efficiency of photoelectric conversion is due to the direct-gap structure of this semiconductor.

When preparing devices based on narrow-gap semiconductors, one major problem concerns providing high quality of the semiconductor's surface and interfaces: diminishing the rate of surface recombination, density of surface states and the built-in charge which negatively affect electrical and photoelectric characteristics of the structures. In the case of MCT, there is an important factor of low stability of the material because of high sensitivity of its structure to external physical, chemical, and thermal effects resulting from a weak chemical bond Hg–Te. Such sensitivity significantly complicates passivation of the MCT surface.

The simplest method of passivating a semiconductor surface is to form a native oxide layer. Since thermal oxidation is not applicable to such sensitive semiconductor as HgCdTe, the technologies of its oxidation started developing with the

[1]Rzhanov Institute of Semiconductor Physics, Siberian Branch, Russian Academy of Sciences, Novosibirsk, Russia; *erzakirov@isp.nsc.ru. Original article submitted November 1, 2018; revised December 26, 2018; accepted February 22, 2019.

methods of electrolytic anodizing [1-3] and RF plasma oxidation [4, 5], the latter providing relatively smaller values f the built-in charge and the density of surface states at the interface. However, the MCT oxidation process itself is accompanied by structure distortions in its near-surface region, and the resulting oxide exhibits weak dielectric properties. Current methods of passivation of the interfaces of MCT based structures imply deposition of dielectrics such as SiO_2 [6-8], Si_3N_x [9], ZnS [10, 11], and Al_2O_3 [12, 13]; however, this process may be accompanied by heating the substrate and mixing its material with the deposited material. In this regard, it is proposed to use the native MCT oxide only as an intermediate layer or as an interface with the semiconductor to protect the latter during the subsequent deposition of the main dielectric. The thinnest possible oxide layer should minimize the distortion of the surface structure of the semiconductor during the oxidation. As we previously showed in [14], a thin layer (~ 1 nm) of native oxide can significantly stabilize the MCT surface during its heating in vacuum and depositing a dielectric or metal layer.

One of the most promising methods of precision and reproducible oxidation of materials is ultrahigh vacuum method of dry oxidation in a glow discharge plasma, which was previously tested for InAs [15, 16]. It is assumed that the approach of combining preliminary passivation and stabilization of the MCT surface by ultrathin native oxide with subsequent deposition of the main dielectric will significantly improve electrophysical and photoelectric parameters of prepared MCT based structures.

The present work is the first study of the kinetics of formation of protective ultrathin (less than 10 nm) native oxide layers on the HgCdTe surface in a glow discharge oxygen plasma. Chemical composition and oxide thickness at initial oxidation stages were determined by the XPS method without using destructive methods of layer-by-layer analysis.

EXPERIMENTAL

Studied material. The object of study is variband heteroepitaxial cadmium mercury telluride ($Hg_{1-x}Cd_xTe$) grown on a silicon substrate; this material possesses electron-type conductivity ($n = 5 \cdot 10^{14}$ cm^{-3}) with volume composition $x = 0.4$ and increasing composition x up to 0.5 at the surface (the thickness of the transition surface layer is about 0.2 μm) [17].

Preliminary preparation of the sample. The formation of ultrathin layers on a semiconductor surface imposes special requirements on the purity and surface relief of original samples. Also, stoichiometry of the multicomponent semiconductor in the subsurface region requires special attention. In this regard, the MCT samples were chemically treated for 30 min in ammonium hydroxide, then thoroughly washed in isopropyl alcohol, and loaded into a vacuum chamber. As a result, native MCT oxide and atmospheric hydrocarbon contamination were removed from the surface with minimal distortions in the stoichiometry of the initial material [14].

No longer than 5 min after the chemical treatment, the samples were placed into the loading chamber of the Surface Science Center SSC RIBER vacuum unit evacuated out to 10^{-7} Torr.

Oxidation in glow discharge plasma. The oxidation process was carried out directly in a module of the unit for surface chemical analysis which allowed us to control the chemical composition of the sample's subsurface region immediately after each treatment cycle in the plasma without transporting it to the laboratory atmosphere. Glow discharge in direct current was ignited in an ultrahigh vacuum chamber equipped with an oil-free pumping system, a system of pure gas inlet, pressure sensors over the range of $1 \cdot 10^{-11}$ – 760 Torr, and vacuum current leads. The glow discharge was not confined within the walls of the vacuum chamber and burned in the free space of the camera. High purity O_2 gas ALPHAGAZ No. 45 was used.

A discharge voltage of 500 V at a gas pressure of 0.15 Torr provides a clear even plasma glow without sparks from the aluminum cathode. The sample was placed behind the solid anode to keep its surface safe from being directly bombarded by plasma ions.

Chemical composition and structure of oxide films. The chemical composition of the subsurface region was studied and the thickness of the formed layer at various oxidation stages was measured using X-ray photoelectron spectroscopy (XPS) on a RIBER unit of the Surface Science Center. The XPS spectra were excided by non-monochromatic

radiation AlK_α with an energy of 1486.6 eV (the source power was 300 W, the X-ray beam diameter was ~ 5 mm). All spectra were obtained at the analyzer resolution $\Delta E = 0.7$ eV corresponding to the Au4$f_{7/2}$ line width at a half height of 1.31 eV. The spectrometer was calibrated for Cu2$p_{3/2}$, Cu3$p_{3/2}$, and Au4$f_{7/2}$ lines to ensure the measurement of the photoelectron energy with an accuracy of at least 0.1 eV. The registration angle for signal electrons was 20° relative to the normal to the sample surface.

The XPSPEAK41 software was used to separate the overlapping photoelectron peaks into individual components fitted by a mixture of Gaussian and Lorentz functions.

The ratio of component concentrations in the subsurface region of the sample was calculated from the ratio of intensities of the corresponding XPS peaks taking into account relative sensitivity factors according to the equation $n_1/n_2 = I_1S_2/I_2S_1$, where I is the integral intensity of the photoelectron peak; S is the relative sensitivity factor of the corresponding chemical element. Accordingly, the element ratio in a multicomponent substance can be expressed as $C_x = n_x/\sum_i n_i = (I_x/S_x)/\sum_i(I_i/S_i)$. Relative sensitivity factors for tellurium and mercury are 4.0 and 2.11, respectively [18], and those for cadmium and oxygen with respect to tellurium were experimentally refined by reference samples CdTe and TeO_2 and were taken to be 2.17 and 0.45, respectively.

The total thickness of obtained oxide films was measured by the XPS method using the decrease of the intensity of the integrated peak Te3$d_{5/2}$ corresponding to Te^{2-} in the composition of the substrate, assuming that the photoelectron intensity attenuates exponentially according to the equation $d_{ox} = \lambda\cos\Theta\cdot\ln(I_{s0}/I_s)$, where λ is the inelastic mean free path of Te3$d_{5/2}$ electrons in the oxide film (1.9 nm) [19]; Θ is the emission angle of registered electrons with respect to the normal to the sample surface (20°); I_{s0} is the integral intensity of the Te3$d_{5/2}$ peak (572.8 eV) of the original surface of the non-oxidized MCT sample; I_s is the integral intensity of the Te3$d_{5/2}$ peak (572.8 eV) of the oxidized sample.

The shifts of spectral lines due to the changes in the surface potential of the sample and/or its chemical state were measured relative to the uniquely identified Te3$d_{5/2}$ line with an energy of 572.8 eV corresponding to tellurium atoms in the substrate.

RESULTS AND DISCUSSION

Fig. 1*a* selectively presents X-ray photoelectron lines Te$d_{5/2}$ recorded immediately after the sample was loaded into the chamber and during its plasma treatment for 1 min, 8 min, 45 min, 120 min, and 300 min. The spectrum of the original sample after chemical treatment contains a single-component peak Te3$d_{5/2}$ with a binding energy of 572.8 eV and the full width at half maximum (FWHM) of 1.6 eV, which corresponds to tellurium in the oxidation state 2– in compounds with cadmium and mercury. The spectrum shows that no natural oxide tellurium is present on the surface. Therefore, it can be assumed that the sample surface does not oxidize during the loading (Fig. 1*a*, *1*) as well as during the maintenance in an oxygen atmosphere at a pressure of 0.15 Torr for 1 h without plasma activation (the spectrum is identical to that of the original sample within the measurement error). After the first cycle of 1 min plasma treatment, the spectrum shows an additional peak Te3$d_{5/2}$ with a binding energy of 576.1 eV and the FWHM of 1.9 eV corresponding to the oxidized Te^{4+} state. At the same time, the Cd3$d_{5/2}$ peak at 405.1 eV broadens from 1.29 eV to 1.46 eV (Fig. 1*b*). With such a small change in the binding energy (< 0.1 eV) of the Cd3$d_{5/2}$ line due to partial substitution of Cd–Te bonds by Cd–O bonds, the exact decomposition of the peak into components is not possible in the present experimental conditions; however, the formation of the oxide component of Cd^{2+} is confirmed by the reduction of the Auger parameter α of cadmium by 1.5 eV [18]. Similarly, the replacement of Hg–Te bonds by Hg–O bonds is associated with a shift towards higher binding energies and slight broadening of the Hg4$f_{7/2}$ line with the initial binding energy of 100.2 eV and the FWHM equal to 1.31 eV (Fig. 1*c*).

The oxygen line that occurs in the spectrum during the oxidation (Fig. 1*d*) is a combination of two core electron peaks at 530.3 eV and 531.8 eV with half widths equal to 1.75 eV and 1.78 eV, respectively. Higher (530.3 eV) and lower (531.8 eV) intensity peaks correspond to O^{2-} and O^- states, respectively. According to some studies [20], the splitting of the

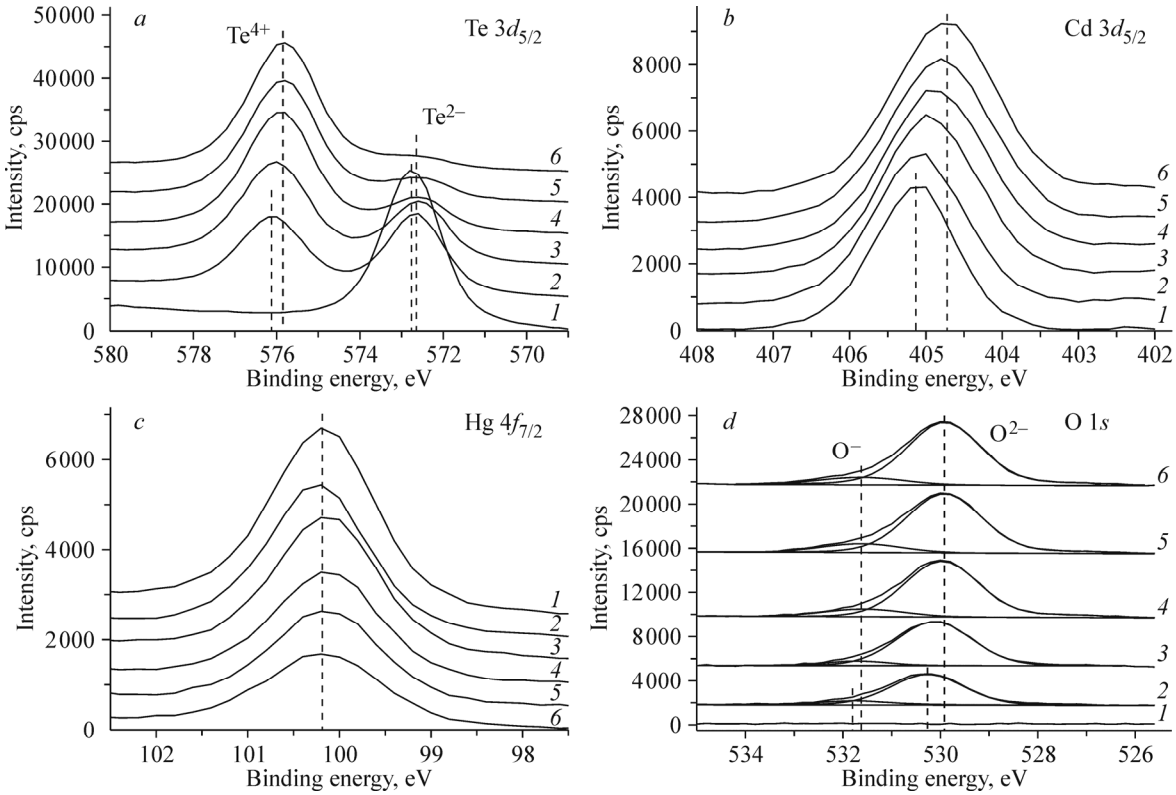

Fig. 1. Evolution of Te3$d_{5/2}$ (*a*), Cd3$d_{5/2}$ (*b*), Hg4$f_{7/2}$ (*c*), and O1*s* (*d*) photoelectron lines during the MCT oxidation in a glow discharge oxygen plasma: original surface (*1*); 1 min, 8 min, 45 min, 120 min, and 300 min of oxidation (*2*-*6*).

O1*s* level into these two states is due to the mixing of ionic and polar covalent bonds. In this case, the degree of ionicity of the oxygen–metal bond in the oxide can be determined from the ratio of intensities of respective components. Thus, it was calculated from the ratio of experimentally obtained areas under the line of O1*s* components corresponding to O^{2-} and O^{-} states that the degree of ionicity of the bond between the oxygen and MCT components exceeds 90%. However, if calculated theoretically according to Pauling's equation [21], the degree of ionicity of Te–O, Cd–O, and Hg–O bonds does not exceed 60%. According to other studies [22], the occurrence of the O^{-} state is due to the fact that oxygen has a lower coordination number than that in its ordinary state rather than to due to chemical bonding. This fact, in turn, results from the presence of defects (oxygen vacancies) in the oxide structure [23-25]. Thus, it is assumed that there is one oxygen vacancy per an oxygen atom in the state O^{-}, the lack of oxygen in the MCT oxide is ~10%, and it does not explicitly depend on the oxidation time in a glow discharge plasma.

The series of spectra recorded after each MCT oxidation cycle (Fig. 1) shows that chemical bonds in the substrate components undergo changes throughout the experiment while the components gradually transform into the oxidized state. The Te3$d_{5/2}$ line is characterized by a monotonic increase of the oxidized tellurium fraction and a shift of the corresponding peak towards lower binding energies to reach 0.4 eV at the final oxidation stage (300 min). The maximum FWHM value of 1.62 eV for the Cd3$d_{5/2}$ line is observed already after 60 min of the sample oxidation, but the line continues shifting until 300 min of oxidation to reach the value of 0.4 eV. After the initial shift in the direction of high binding energies, the Hg4$f_{7/2}$ peak gradually shifts in the process of sample oxidation to the opposite direction so that the difference between the positions corresponding to 1 min and to 300 min of oxidation was ~0.2 eV and the FWHM increased up to 1.52 eV. The O1*s* line during the experiment shifts by 0.35 eV towards lower binding energies, while the half width remains virtually unchanged; however, the distance between the O^{2-} and O^{-} peaks increases from 1.5 eV to 1.7 eV.

The observed shift of the lines of the oxidized sample surface relative to those of the substrate can be explained by a change in the surface potential due to a negative charge accumulated at the interface and/or in the volume of the oxide. A relatively small shift of mercury lines indicates that the ratio of these atoms in the MCT oxide layer is small and that the decreasing mercury signal is formed mainly in the non-oxidized substrate. Accordingly, a small (0.1 eV) shift of the O^- peak towards lower binding energies suggests that the oxygen-depleted oxide layer is located near the border with the MCT and that oxidation occurs mainly due to the diffusion of oxygen to the semiconductor–oxide interface.

The spectra shown in Fig. 1*a* were used to reveal the kinetics of MCT oxidation in a glow discharge oxygen plasma presented in Fig. 2. According to Mott–Cabrera [26] and Hauffe–Ilschner [27] theories that describe the growth of ultrathin protective oxide films and using known generalizations of experimental data on low-temperature oxidation of metals [28], the experimentally obtained MCT oxidation kinetics can be characterized as follows.

In general, the oxidation process is related to electron and ion currents (equal in magnitude and opposite in direction) through the formed insulating oxide. In this case, the electron current is due to the quantum-mechanical effect of electron tunneling from the oxidized substance to the oxygen adsorbed on the surface, and this current does not initially limit the reaction rate. As the oxide thickness increases, this current decreases exponentially. Thus, at the early oxidation stages, the rate of the process is limited by the ion current caused by diffusion and the electric field at the semiconductor–oxygen interface. Under relatively low (room) temperatures, the contribution of diffusion is negligible, and the main contribution is due to the so-called Mott potential, i.e. the electric potential difference formed by positive ions of the oxidized substance at the semiconductor–oxide interface and by negative oxygen ions at the oxide–oxygen interface. According to Cabrera and Mott, the oxidation kinetics in these conditions is described by an inverse logarithmic law $1/d = A - k_1 \cdot \ln t$ [26]. When the oxide reaches certain thickness (2-3 nm), the electron tunneling current becomes the limiting factor and, according to Hauffe and Ilschner, the thickness becomes a logarithmic function of the oxidation time $d = k_2 \cdot \ln(\alpha t + 1)$ [27]. This transition from one mechanism to another is clearly seen in the experimental dependence of the MCT oxide thickness on the oxidation time which is approximated by the $1/d = 0.74 - 0.11 \ln t$ function at the initial stage ($d < 3$ nm) and by the $d = 0.72 \ln(1.37t + 1)$ function at the next stage ($d > 2$ nm) (Fig. 2). The thickness range of 2-3 nm is a transition region where the electron tunneling current and the ion current are close in magnitude, and the maximum oxide thickness is limited by the thickness of ~5 nm, which is typical for the oxidation of metals in the limiting conditions of an electron tunneling current [27, 28].

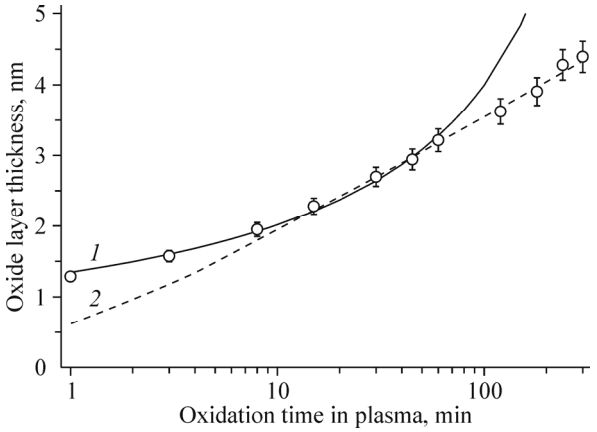

Fig. 2. Kinetics of MCT oxidation in a glow discharge oxygen plasma. Discharge voltage $U = 500$ V, chamber pressure $P = 0.15$ Torr; experimental data (dots): approximation of the early oxidation stage by the Mott–Cabrera inverse logarithmic law $1/d = 0.74 - 0.11 \cdot \ln t$ (curve *1*), approximation of the next stage by the Hauffe–Ilschner direct logarithmic law $d = 0.72 \cdot \ln(1.37t + 1)$ (curve *2*).

The ternary diagram in Fig. 3 shows the changes in the concentration ratios of tellurium, cadmium, and mercury in the subsurface region calculated as the ratios of total areas under corresponding photoelectron peaks to the sensitivity factors. As can be seen, tellurium is the main component of the growing native MCT oxide, its ratio remains almost unchanged in the oxidation process and approximately equals to that of the original sample. At the same time, the ratio of cadmium in the subsurface region increases while that of mercury decreases. The latter is due to the fact that the Te–Hg bond breaking may result not only in the formation of the Hg–O bond but also in the diffusion of mercury towards the substrate volume through interstices or into vacuum. The contributions of these diffusions cannot be separated by chemical analysis; however, it should be noted that interstitial mercury atoms can form electrically active donor complexes [29], but the analysis of electrophysical characteristics of MIS structures HgCdTe–native oxide–Al_2O_3–Au revealed no significant increase in the concentration of most charge carriers.

Fig. 4 shows the changes in the ratios of subsurface concentrations of oxygen and oxidized tellurium atoms during plasma treatment. This dependence has an inflection point corresponding to the thickness of the oxide layer of ~2 nm and

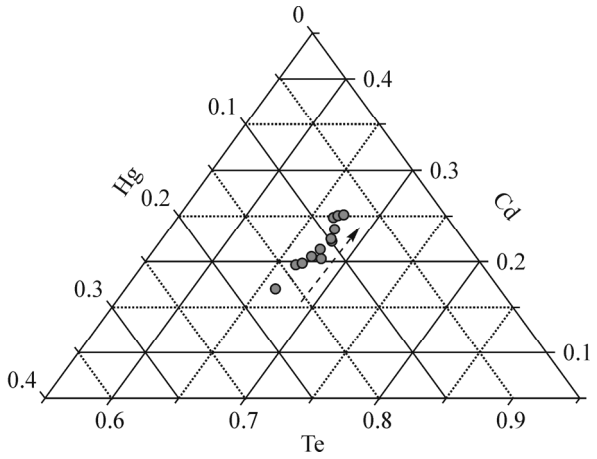

Fig. 3. Ternary diagram of concentration ratios of tellurium, cadmium, and mercury atoms in the subsurface region of the structures formed in a glow discharge oxygen plasma. The arrow indicates the direction of the increase of oxidation time in the plasma.

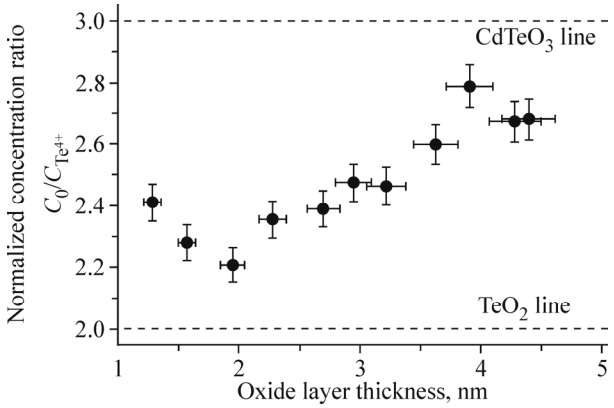

Fig. 4. Normalized concentration ratio of oxygen and tellurium Te^{4+} atoms in the subsurface region of native MCT oxide formed in a glow discharge oxygen plasma. Dashed lines indicate concentration ratios corresponding to the predominant formation of tellurium oxide TeO_2 or cadmium tellurite $CdTeO_3$.

indicating that the oxidation mechanism changes when this thickness exceeds 2 nm. First monolayers of native MCT oxide, in the absence of the drift of metal cations, seem to be formed due to almost complete oxidation of surface tellurium, cadmium, and mercury (or rather the remainder of the latter after its diffusion into vacuum and into the bulk of the substrate). At the early stages, which we describe using the Mott–Cabrera theory, the concentration ratio of oxygen to oxidized tellurium decreases and approaches the value of 2.0 (TeO_2 is mainly formed on the MCT surface) to indicate a lower rate of cadmium and mercury oxidation compared to tellurium. After the thickness of native MCT oxide reaches 2 nm, this ratio increases again, since the direct oxidation of tellurium becomes limited by the drift of its cations to the semiconductor–oxide interface.

The obtained experimental data generally agree with current concepts of MCT oxidation. Thus, it was noted in [3, 30-32] that the oxidized form of tellurium prevails in the composition of native MCT oxide (its ratio relative to cadmium and mercury is ~60%). At the same time, there is uncertainty in establishing exact composition of the oxide layer, which may include compounds such as TeO_2, CdO, $CdTeO_3$, $CdTe_2O_5$, HgO, $HgTeO_3$, and $HgTe_2O_5$ [3, 31, 33]. This uncertainty is caused by the features of the methods of destructive layer-by-layer chemical analysis and the methods of photoelectron spectroscopy. Nevertheless, TeO_2, $CdTeO_3$, and $HgTeO_3$ are the most stable and probable forms in the cases of anodizing in electrolyte [2, 33, 34] and in oxygen plasma [32, 35].

The conclusion that MCT oxide growth is mainly due to the drift of oxygen anions into the oxidized material is consistent with the data reported in [36] which were obtained by examining the composition profile of MCT anodic oxide containing "marked" layers and the data of work [3] suggesting the presence of oxygen vacancies near the oxide–HgCdTe interface. From the point of view of electrophysics, such mechanism of oxide growth (when its boundary with the semiconductor is shifted inside the original semiconductor surface) results in a higher-quality interface than the one formed by the original surface with defects and/or impurities. However, despite relatively low diffusion rate of tellurium and cadmium as compared to oxygen, the authors of [32, 37] observed high content of cadmium in its native MCT oxide and/or near the native oxide– MCT interface, which is also consistent with our result.

Another important feature mentioned both in [31, 35] and in the present work is mercury depletion at the native oxide–HgCdTe interface; it was also reported in [31] that the depth of the depleted semiconductor region depends on the thickness of the anodic oxide but does not exceed 15-20 nm while the oxide thicknesses exceeds 100 nm. It is known that mercury vacancies are electrically active and act as acceptors. It is because of the oxidation effect on the composition and structure of the boundary semiconductor region that we paid great attention to the formation of ultrathin oxide films on MCT.

CONCLUSIONS

The initial stages of low-temperature HgCdTe oxidation in a glow discharge oxygen plasma were first studied by the XPS method, the data on chemical composition of oxide films on the MCT surface, their kinetics, and growth mechanism were obtained.

The following features and regularities were established:

1. The very first stage of the interaction of oxygen with a preliminary cleaned MCT surface is associated with an oxidation of all three components of the substrate. The subsurface concentration of mercury decreases, since a part of mercury atoms leave the surface.

2. The kinetics of MCT oxidation in an oxygen plasma contains two characteristic regions and is described by the laws $1/d = 0.74 - 0.11\ln t$ for the thicknesses below ~3 nm and by $d = 0.72\ln(1.37t + 1)$ for the thicknesses above ~2 nm. At early stages, the oxidation process is limited by the current of ions drifting in an electric field created by the potential difference at the semiconductor–oxide and oxide– oxygen interfaces. At later stages, it is limited by the electron tunneling current from the substrate to the oxygen adsorbed on the surface, which is decreased exponentially with increasing thickness of the oxide layer.

3. The growth of the film occurs mainly due to the drift of oxygen anions into the oxidized material, and the oxide layer near the semiconductor–oxide interface is characterized by oxygen deficiency.

4. Qualitatively, the composition of native MCT oxide does not depend on the oxidation method (wet anodization, oxidation in a RF plasma). The main component of the native oxide film is oxidized tellurium in the form of tellurium oxide and cadmium tellurite. As the film thickness increases, the ratio of oxidized cadmium increases and the ratio of mercury decreases due to its predominant diffusion into vacuum during the oxidation process.

The work demonstrates a fundamental possibility of precise formation of tunnel-thin films of native MCT oxide on its surface in a glow discharge oxygen plasma at room temperature. Oxygen plasma can be used for preliminary stabilization of the surface before applying a gate or protective dielectric.

The results of the study are of practical interest in terms of solving the problem of MCT surface passivation.

ACKNOWLEDGMENTS

The authors are grateful to M.V Yakushev for providing the MCT samples.

FUNDING

This work was supported by the Russian Foundation for Basic Research, project No. 13-07-12151-ofi-m.

CONFLICT OF INTERESTS

The authors declare that they have no conflict of interests.

REFERENCES

1. P. C. Catagnus and C. T. Baker. U.S. Patent No.3,977,018, **1976**.
2. Y. Nemirovsky and E. Finkman. *J. Electrochem. Soc.*, **1979**, *126*, 768.
3. T. S. Sun, S. P. Bucher, and N. E. Byer. *J. Vac. Sci. Technol.*, **1980**, *17*, 1067.
4. Y. Nemirovsky and R. Goshen. *Appl. Phys. Lett.*, **1980**, *37*, 813.
5. Y. Nemirovsky, R. Goshen, and I. Kidron. *J. Appl. Phys.*, **1982**, *53*, 4888.
6. J. A. Wilson, V. A. Cotton, J. Silberman, D. Laser, W. E. Spicer, and P. Morgen. *J. Vac. Sci. Technol. A*, **1983**, *1*, 1719.
7. V. N. Ovsyuk, V. V. Vasil′ev, and Yu. P. Mashukov. *Semicond.*, **2000**, *34*, 794.
8. A. V. Sorochkin, V. S. Varavin, A. V. Predein, I. V. Sabinina, and M. V. Yakushev. *Semicond.*, **2012**, *46*, 535.
9. J. Zhang, G. A. Umana-Membreno, R. Gu, W. Lei, J. Antoszewski, J. M. Dell, and L. Faraone. *J. Electron. Mater.*, **2015**, *44*, 2990.
10. R. K. Bhan, V. Srivastava, R. S. Saxena, L. Sareen, R. Pal, and R. K. Sharma. *Infrared Phys. Technol.*, **2010**, *53*, 404.
11. P. Xu, G. Xu, K. Chu, N. Wang, Q. Zhou, Y. Tang, K. Zhang, and X. Li. *Proc. SPIE*, **2013**, *8907*, 890742.
12. V. Damnjanovic and J. M. Elazar. 27th International Conference on Microelectronics Proceedings. **2010**, 131.
13. R. Fu, J. Pattison, A. Chen, and O. Nayfeh. *Proc. SPIE*, **2012**, *8353*, 835321.
14. V. G. Kesler and E. R. Zakirov. 15th International Conference of Young Specialists on Micro/Nanotechnologies and Electron Devices (EDM) Proceedings. **2014**, 33.
15. V. G. Kesler. *J. Struct. Chem*., **2011**, *52*(*Suppl. 1*), 153.
16. V. G. Kesler, A. A. Guzev, A. P. Kovchavtsev, A. V. Tsarenko, and Z. V. Panova. *Optoelectron. Instrument. Proc.*, **2014**, *50*, 87.
17. Yu. G. Sidorov, S. A. Dvoretskii, V. S. Varavin, N. N. Mikhailov, M. V. Yakushev, and I. V. Sabinina. *J. Semicond.*, **2001**, *35*, 1045.
18. C. D. Wagner, W. M. Riggs, L. E. Davis, and J. F. Moulder. Handbook of X-ray Photoelectron Spectroscopy. Perkin-Elmer Corporation: USA, Eden Prairie, Minnesota, **1979**.

19. NIST Electron Inelastic-Mean-Free-Path Database. Version 1.2. National Institute of Standards and Technology, Gaithersburg, USA.
20. L. Q. Wu, Y. C. Li, S. Q. Li, Z. Z. Li, G. D. Tang, W. H. Qi, L. C. Xue, X. S. Ge, and L. L.Ding. *AIP Adv*., **2015**, *5*, 097210.
21. S. S. Batsanov. Experimental foundations of structural chemistry. University Press: Russia, Moscow, **2008**.
22. J.-C. Dupin, D. Gonbeau, P. Vinatier, and A. Levasseur. *Phys. Chem. Chem. Phys.*, **2000**, *2*, 1319.
23. M. Naeem, S. K. Hasanain, M. Kobayashi, Y. Ishida, A. Fujimori, S. Buzby, and S. I.Shah. *Nanotechnology*, **2006**, *17*, 2675.
24. Y. B. Lin, Y. M. Yang, B. Zhuang, S. L. Huang, L. P. Wu, Z. G. Huang, F. M. Zhang, and Y. W. Du. *J. Phys. D: Appl. Phys.*, **2008**, *41*, 195007.
25. P. Zhang, C. Gao, F. Lv, Y. Wei, C. Dong, C. Jia, Q. Liu, and D. Xue. *Appl. Phys. Lett.*, **2014**, *105*, 152904.
26. N. Cabrera and N. F. Mott. *Rep. Progr. Phys.*, **1948**, *12*, 163.
27. K. Hauffe and B. Z. Ilschner. *Elektrochem.*, **1954**, *58*, 382.
28. A. T. Fromhold and E. L. Cook Jr. *Phys. Rev.*, **1967**, *158*, 600.
29. N. Berchenko, I. Izhnin, V. Yudenkov, M. Pociask, and V. Yakovyna. *Surf. Interface Anal.*, **2010**, *42*, 902.
30. C. Stahle, C. R. Helms, H. F. Schaake, R. L. Strong, A. Simmons, J. B. Pallix, and C. H. Becker. *J. Vac. Sci. Technol. A*, **1989**, *7*(1989), 474.
31. G. D. Davis, T. S. Sun, S. P. Buchner, and N. E. Byer. *J. Vac. Sci. Technol.*, **1981**, *19*, 472.
32. V. P. Parkhutik, J. M. Martinez-Duart, J. Perriere, A. Climent, Yu. E. Makushok, and J. M. Albella. *Thin Solid Films*, **1991**, *200*, 129.
33. M. Seelmann-Eggebert, G. Brandt, and H. J. Richter. *J. Vac. Sci. Technol. A*, **1984**, *2*, 11.
34. U. Solzbach and H. J. Richter. *Surf. Sci.*, **1980**, *97*, 191.
35. W. H. Makky, A. Siddiqui, and C. H. Tang. *J. Vac. Sci. Technol. A*, **1986**, *4*, 3169.
36. R. L. Strong. *J. Vac. Sci. Technol. A*, **1987**, *5*, 2003.
37. J. A. Silberman, D. Laser, I. Lindau, W. E. Spicer, and J. A. Wilson. *J. Vac. Sci. Technol. A*, **1983**, *1*, 1706.